Electronic supplementary information (ESI)

Amorphous Lanthanum-Iridium Solid Solution with Open Structure for Efficient Water Splitting

Wei Sun[a], Chenglong Ma[b], Xinlong Tian[c], Jianjun Liao[a], Ji Yang[b], Chengjun Ge[a] and Weiwei Huang[a,*]

a. Key Laboratory of Agro-Forestry Environmental Processes and Ecological Regulation of Hainan Province, College of Ecology and Environment, Hainan University, 58 Renmin Road, Haikou 570228, P.R. China.

b. State Environmental Protection Key Laboratory of Environmental Risk Assessment and Control on Chemical Processes, School of Resources and Environmental Engineering, East China University of Science and Technology, 130 Meilong Road, Shanghai 200237, P.R. China.

c. State Key Laboratory of Marine Resource Utilization in South China Sea, Hainan University, 58 Renmin Road, Haikou 570228, P.R. China.

*Weiwei Huang: huang05106114@163.com

METHODS

Material preparation

La-Ir NF: The substrate of La(OH)$_3$ was prepared via hydrothermal synthesis process. Specifically, 5 mL of 0.1 M lanthanum nitrate (La(NO$_3$)$_3$; analytically pure, Shanghai Ling Feng Chemical Reagent Co.,Ltd) solution was added into 20 mL of 0.1 M sodium hydroxide (NaOH; analytically pure, Shanghai Ling Feng Chemical Reagent Co.,Ltd), then the mixture was transferred into a 40-mL Teflon-lined pressure vessel and placed in an oven to heat the solution to 130 °C for 720 min. The precipitates were suction-filtered and washed with deionized water twice to remove the impurities. The remaining solid on the filter membrane was dried in an oven at 60 °C for at least 30 min. Subsequently, 30 mg of the prepared La(OH)$_3$ solid was added into 20 mL 0.1M NaOH solution and the mixture was ultrasonicated for at least 30 min to ensure that it was homogenized. Then 2 mL of 20 mg/L iridium (IV) chloride (H$_2$IrCl$_6$·6H$_2$O; analytically pure, TCI (shanghai) Development Co.,Ltd) precursor was added into the solution. And the samples were transferred into a 40 mL Teflon-lined pressure vessel and ultrasonicated for approximately 10 min to form a homogeneous solution. The vessel reactors were placed in an oven and heated at 150 °C for 720 min. The precipitates were suction-filtered and washed with deionized water twice. The remaining solid on the filter was dried at 60 °C for at least 30 min. Finally, the obtained powders are annealed at 400 °C for 6 h.

Crystalline and amorphous IrO$_2$: 3 mL of 20 mg/L iridium (IV) chloride (H$_2$IrCl$_6$·6H$_2$O) precursor was added into 20 mL of 0.1 M NaOH solution. Then, the mixture solution was transferred into a 40 mL Teflon-lined pressure vessel and heated in an oven at 150 °C for 720 min. Subsequent purification process was consistent with the preparation method of La-Ir NF. To prepare crystalline and amorphous IrO$_2$, the iridium oxides solid were annealed respectively at 600 °C and 200 °C for 6 h.

Electrode preparation and Electrochemical Measurements

The electrodes used for the electrochemical measurements were prepared as follows. First, 6 mg of fresh catalyst powder was dispersed into a solution mixed with 1.5 mL of 2:1 v/v isopropanol/water and 15 μL of Nafion. Then the solution was ultrasonicated for approximately 30 min to achieve homogeneity. Next, 7.5 μL of the homogenized solution was deposited on a tailored Ti plate with dimensions of 0.5 cm × 1.5 cm. The Ti plate was etched for 2 h by 10% (wt %) oxalic acid under near boiling conditions. The deposition process was repeated 5 times to obtain a loading weight of approximately 0.2 mg cm^{-2}.

Electrochemical tests were performed in a three electrode system. Here, a saturated calomel electrode (SCE) was employed as the reference, and a polished and cleaned Pt foil with a 1.5 cm × 1 cm reaction area was used as the counter electrode. The electrode potential from the SCE scale was converted into the reversible hydrogen electrode (RHE) scale by calibration with an equation: E (RHE) = E (SCE) + E$_{j=0}$. The over-potential values (η) corrected with the iR were calculated using the following equation: η = E$_{Applied}$ (RHE) − iR − 1.229. The SCE was calibrated with respect to the RHE in the 0.1 M perchloric acid (HClO$_4$, A.R. purity) solutions using a high purity hydrogen saturated electrolyte with a Pt foil as the working electrode. CVs experiments were performed at a scan rate of 1 mV/s, and the average value of the two potentials at which the current crossed zero was recorded as the thermodynamic potential for the hydrogen electrode reaction. The OER determinations were performed in 0.1 M HClO$_4$ solution. The working electrodes were cycled at

least 5 times until the curves overlapped in the CV experiments; then the CV data and polarization curves were recorded at the specified scan rate. The OER activity of prepared materials were determined by potential step chronoamperometry (PSCA). The parameters of PSCA are that the initial potential set on 1.1 V (vs. SCE) and the final potential set on the 1.4 V (vs. SCE), potential step is 5 mV and the duration of each step is 30 seconds.

Materials Characterization

The crystal structure of the catalysts was investigated using powder X-ray diffraction (XRD) equipped with a D/max2550 V apparatus and a Cu-Kα radiation source (λ=1.5406 Å), and the data were recorded from 10 to 80° at the step size of 0.02°. A JEM-2100 transmission electron microscope (TEM) was used to characterize the surface morphology. Compositions of the materials were determined by Energy dispersive X-ray (EDX) spectrometer using a TEAMApollo system. The surface properties of the catalysts were determined via X-ray photoelectron spectroscopy (XPS) using an ESCALAB 250Xi instrument with Al-Kα radiation source at an energy step size of 0.05 eV to obtain high-resolution XPS spectra. The samples were sputter-coated with carbon, and the spectra were calibrated with respect to C-*1s* at the binding energy of 284.6 eV. The X-ray absorption (XAS) data of the samples were recorded at room temperature in transmission mode using ion chambers in the Shanghai Synchrotron Radiation Facility (SSFR, beamline BL14W1, Shanghai) and National Synchrotron Radiation Laboratory (NSRL, beamline BL11U, Hefei), China. In order to keep the sample thickness consistent, the overall mass reach 50 mg by adding LiF. The station was operated with a Si (111) double crystal monochromator. During measurements, the synchrotron was operated at the energy of 3.5 GeV and the current varied between 150and 210 mA.

Morlet wavelet transform

In this work, the following Morlet wavelet model was used:

$$\psi(t) = \frac{1}{\sqrt{2\pi\sigma}} \left(\exp(i\kappa t) - \exp(-\frac{\kappa^2}{2}) \right) \exp(-\frac{t^2}{2\sigma^2})$$

Where κ and σ are the free parameters in program. The resolution between *k*-space and *R*-space is determined by the parameters of κ and σ. In the M-WT, the larger the value of κ, the higher resolution of *R*-space, which will be very close to the EXAFS spectra. In contrary, lowing the value of κ will obtain to a high resolution of *k*-space. In this work, for a high resolution of *R*-space, we used the parameters of κ and σ are the 15 and 1, respectively. For a good resolution of k-space, the parameters are the 7.5 and 0.5, respectively.

Figures

Name	Start BE	Peak BE	End BE	FWHM eV	SF	Atomic %
C-1s	288	284.66	281	1.64	1	6.64
O-1s	539	530.73	526	3.84	2.881	61.54
Ir-4f	71	63.58	54.5	5.85	13.945	13.34
La-3d	842	835.33	828	6.68	32.944	7.55
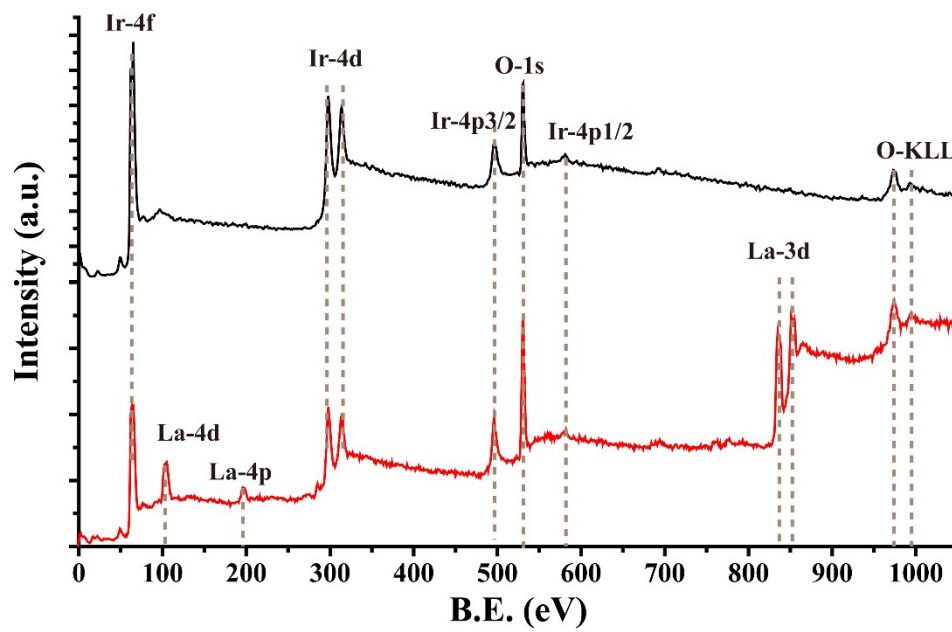
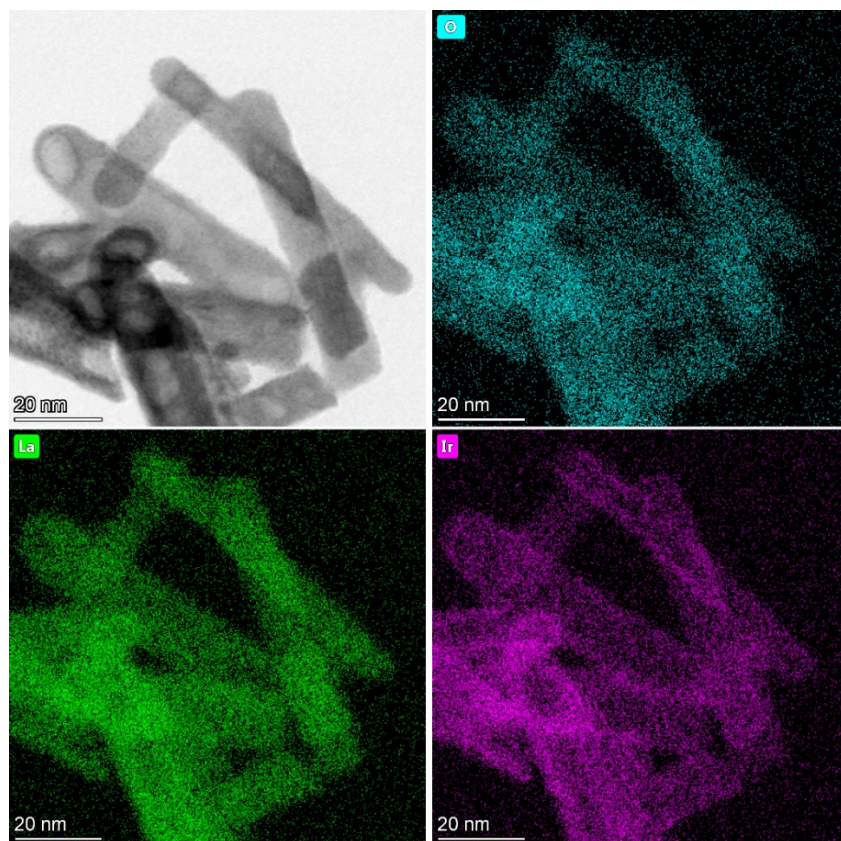**Figure S1.** The over-all XPS spectra of IrO_2-Cry and La-Ir NF. Table lists the surface elements contents of La-Ir NF by XPS.

Figure S2. Elemental mapping analysis of Ir, La, and O atoms in La-Ir NF.
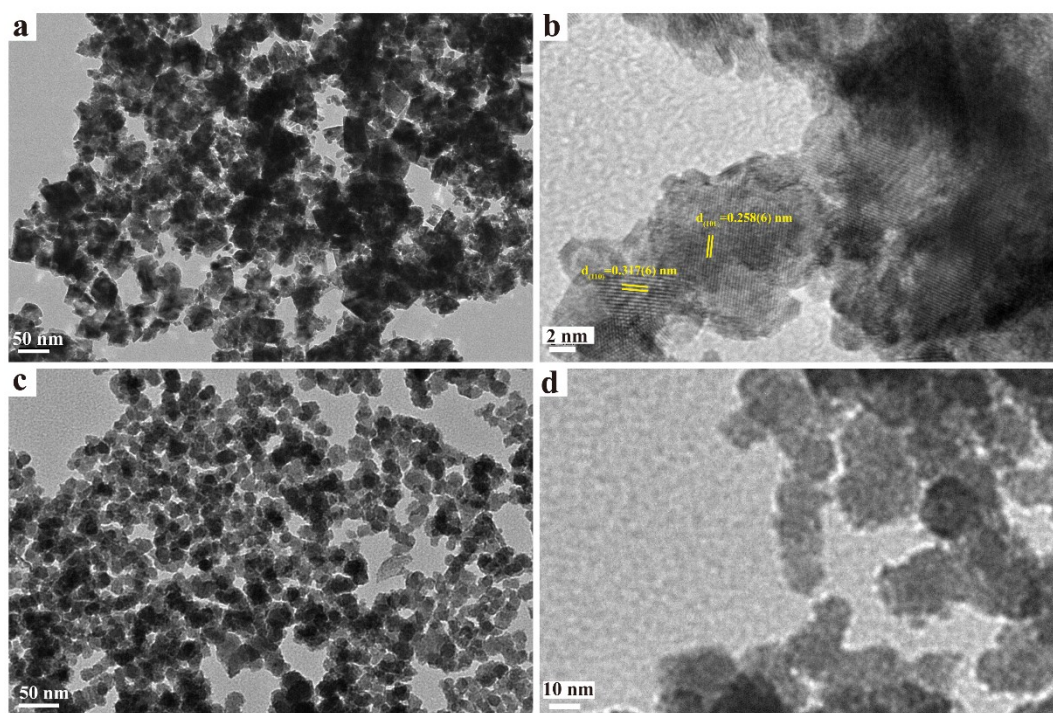
Figure S3. (a) and (b) are the TEM and HRTEM images of IrO$_2$-Cry. The lattice finger of (110) and (101) are marked in the (b). (c) and (d) are the TEM and HRTEM images of IrO$_2$-Am.
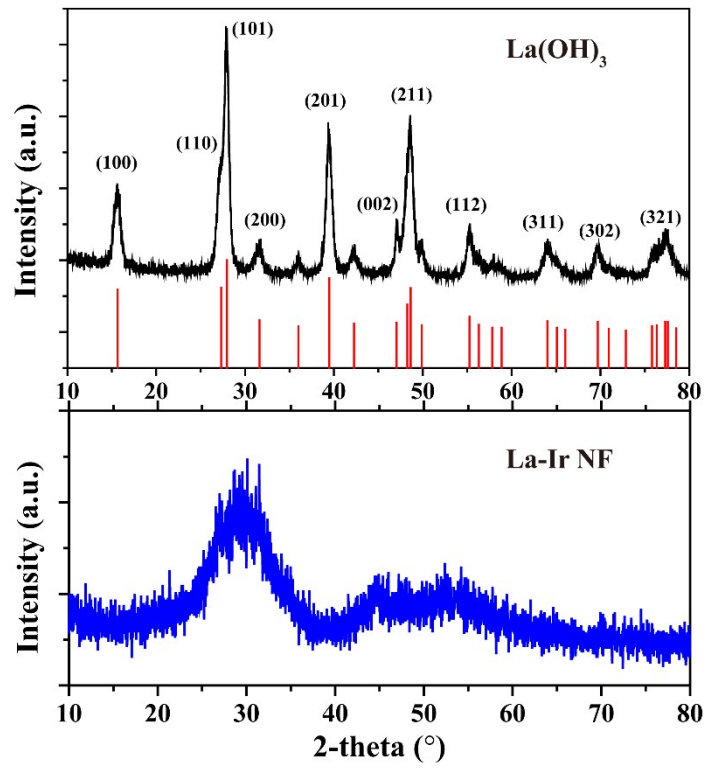
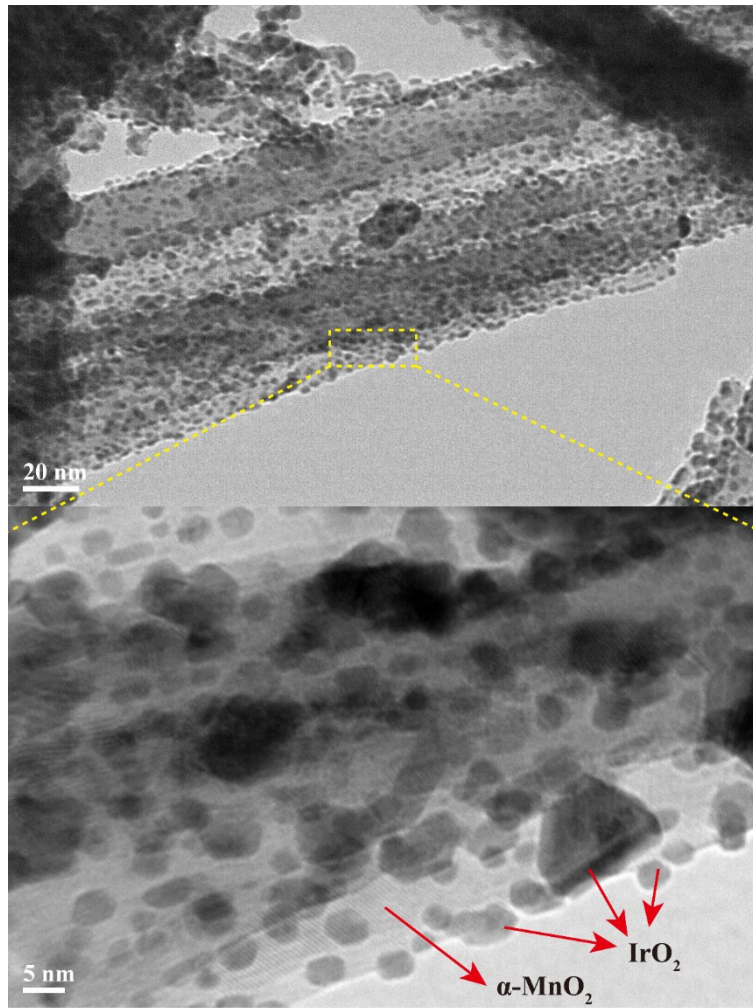**Figure S4.** XRD patterns of La(OH)$_3$ and La-Ir NF.

Figure S5. The TEM and HRTEM images of $IrO_2@\alpha\text{-}MnO_2$. The $IrO_2@\alpha\text{-}MnO_2$ is prepared according to our previous method[1].
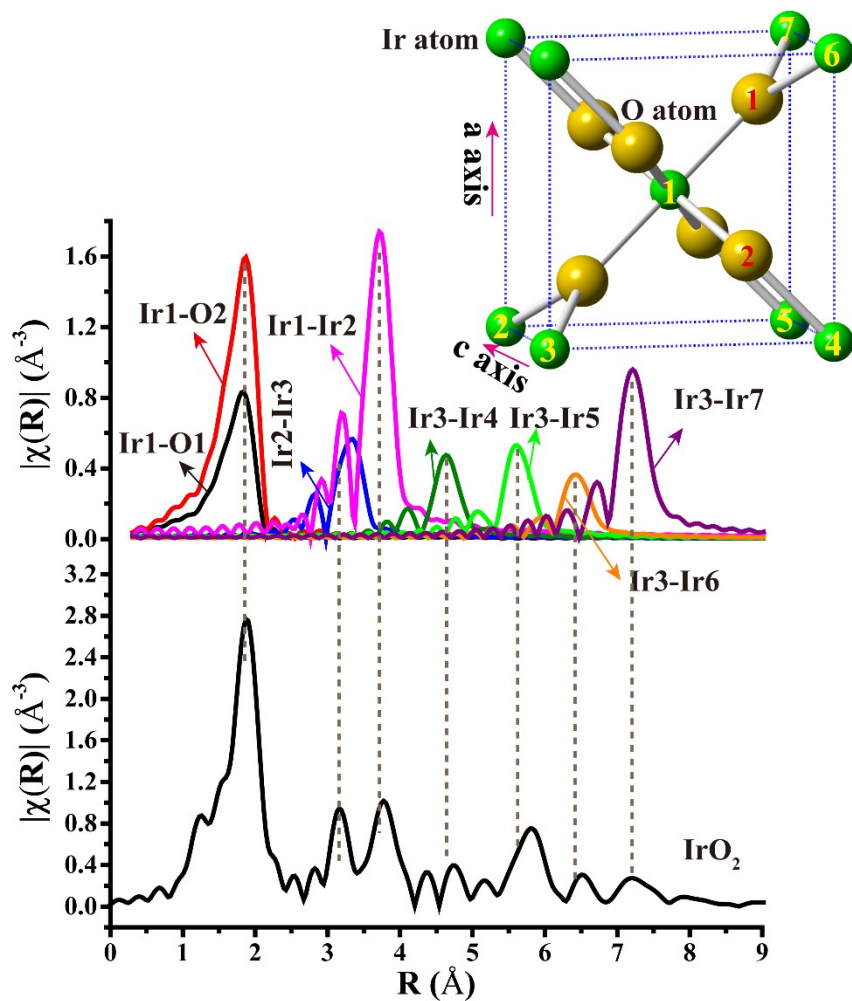
Figure S6. The FT-EXFAS spectra of standard IrO_2. The calculated scattering paths are based from the IrO_2.cif data[2]. IrO_2 parameters are $a=b=4.5051$ Å, $c=3.1586$ Å, space=P42/mnm, Ir-O_2=1.9604 Å; Ir-O_4=1.9988 Å. The bottom FT-EXAFS is the IrO_2-Cry, k range are the 2-14 Å, and be phase corrected.
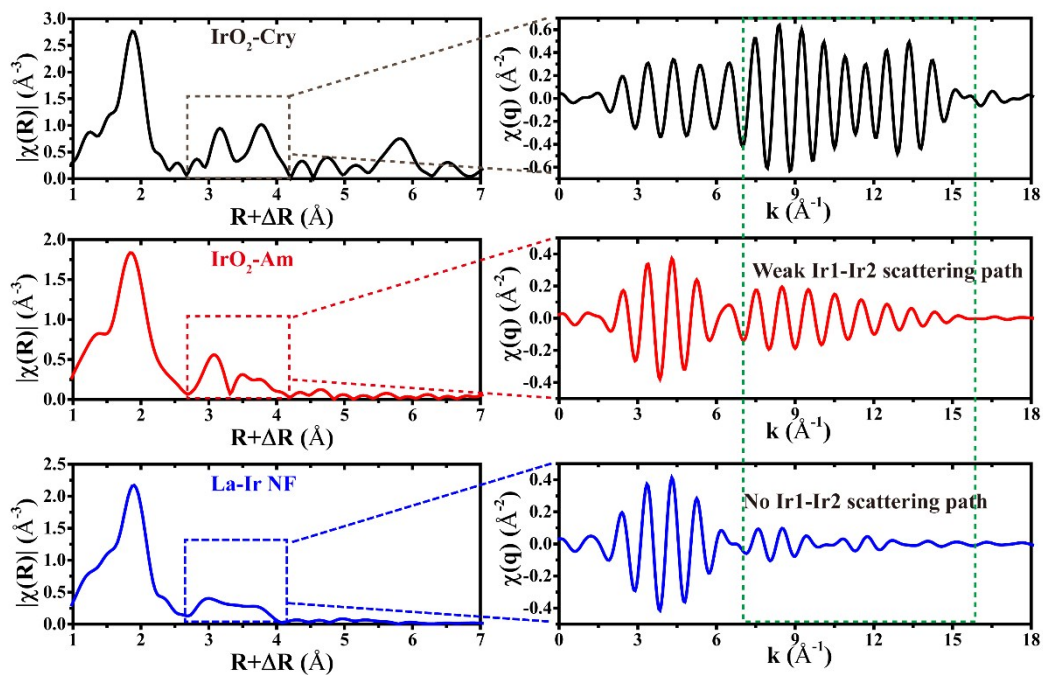
Figure S7. The EXAFS spectra of prepared materials and the k^2-weighted backward Fourier transforms of EXAFS spectra in selected R range of 2.6-4.2 Å.
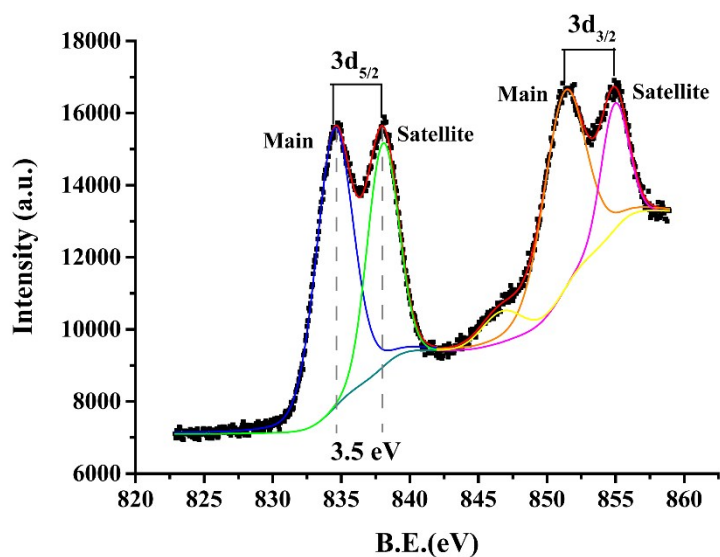

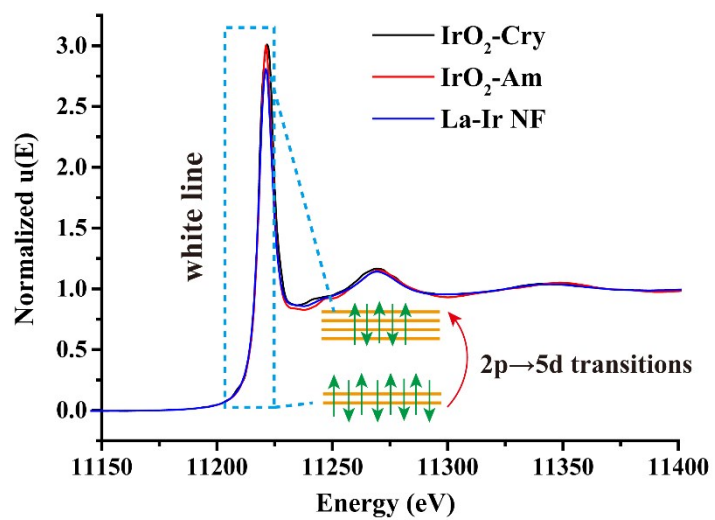**Figure S8.** The La-3d core level XPS of La-Ir NF.

Figure S9. The Ir-L$_{III}$ edge XANES spectra of prepared materials.
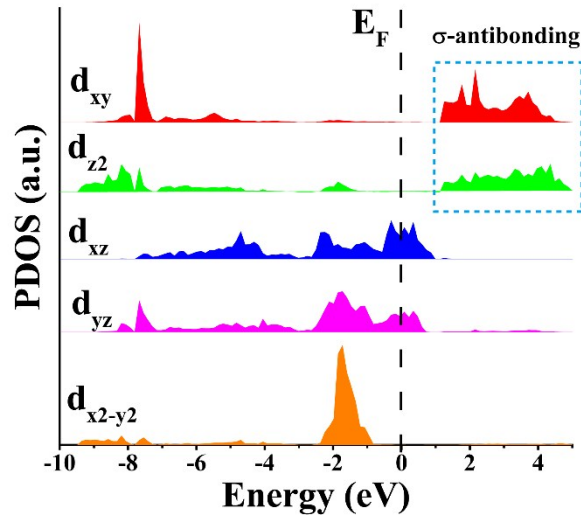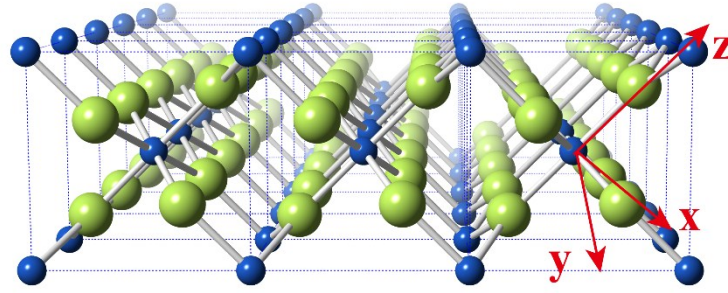
Figure S10. The upper is crystallography of IrO_2 and the bottom is the PDOS of Ir 5d orbitals. The DFT calculations were conducted using the Vienna Ab-initio Simulation Package (VASP)[3, 4]. The projector augmented wave (PAW) method with the generalized gradient approximation (GGA) for the exchange-correlation functional in a form suggested by Perdew, Burke, and Ernzerhof (PBE)[5] was used to calculate the optimized lattice parameters of bulk IrO_2. The coordinates of atoms were allowed to relax, with the residual force components on each atom lower than ~0.05 eV·Å^{-1} atom^{-1}. A ~20 Å of vacuum space was introduced to curtail interactions between the slabs. The spin polarization was set for all of the calculations.DOS was calculated by Gaussian smearing method with the width of 0.1 eV using a denser k-point grid of 3 × 3 × 15 for the 2 × 2 × 1 IrO_2 supercell
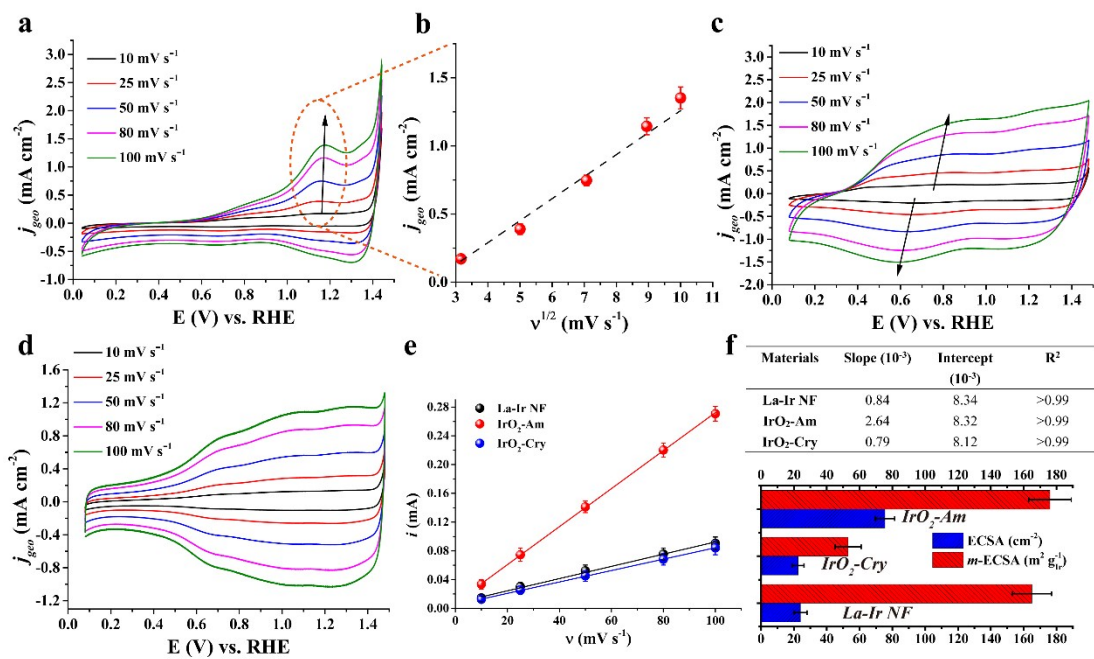
Figure S11. Electrochemical properties of prepared materials. (a) The CV curves of La-Ir NF at different scan rate. (b) The relationship between identified peak current and the $v^{1/2}$. (c) and (d) are the CV curves of IrO_2-Am and IrO_2-Cry, respectively. (e) The relationship between the capacitive current and the scan rate. (f) The linear fitting results in (e) and their corresponding ECSAs.
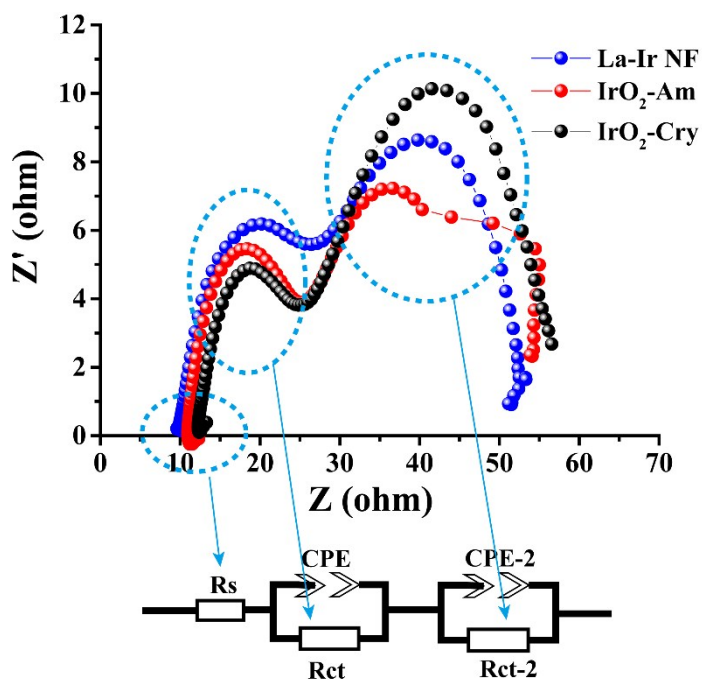

Figure S12. The Nyquist plots of prepared materials by EIS. The equivalent circuit is shown in bottom. The EIS measurements are conducted at 1.25 V vs. SCE with a sinusoidal voltage of 10 mV and a frequency ranging from 10^6 to 1 Hz.
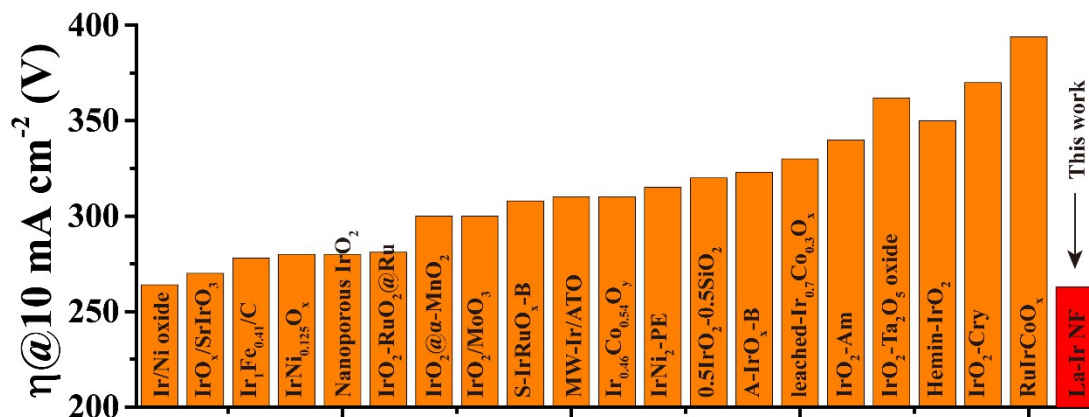
Figure S13. The OER activity comparison of the different IrO_2-based oxides[6-21].
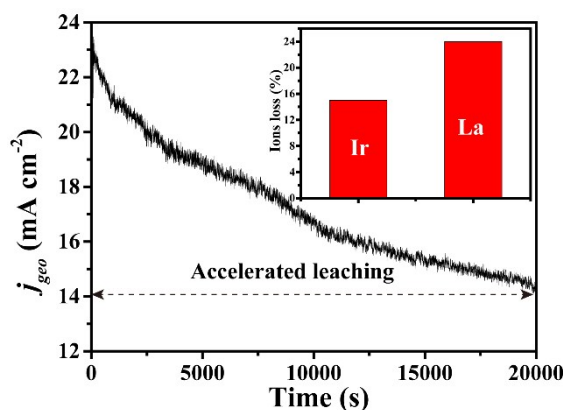

Figure S14. The current-time curves at the 1.60 V vs. RHE by FPA for La-Ir NF. The measurements is conducted in the 0.1 M $HClO_4$, catalyst loading mass was ~0.2 mg cm^{-2} and electrode area was 0.25 cm^2. The insert corresponds to the amount of leaching metal ions deterimined by ICP-AES after the durability test.

References:

1. W. Sun, Z. Zhou, W. Q. Zaman, L.-m. Cao and J. Yang, *ACS Appl. Mater. Interfaces*, 2017, **9**, 41855-41862.

2. A. A. Bolzan, C. Fong, B. J. Kennedy and C. J. Howard, *Acta Crystallogr.*, 1997, **53**, 373–380.

3. G. Kresse and J. Furthmüller, *Computational Materials Science*, 1996, **6**, 15-50.

4. G. Kresse and J. Hafner, *Physical Review B*, 1993, **47**, 558-561.

5. J. P. Perdew, K. Burke and M. Ernzerhof, *Phys. Rev. Lett.*, 1996, **77**, 3865-3868.

6. S.-A. Park, K.-S. Kim and Y.-T. Kim, *ACS Energy Letters*, 2018, **3**, 1110-1115.

7. A. Yu, C. Lee, M. H. Kim and Y. Lee, *ACS Appl. Mater. Interfaces*, 2017, **9**, 35057-35066.

8.   W. Hu, H. Zhong, W. Liang and S. Chen, *ACS Appl. Mater. Interfaces*, 2014, **6**, 12729-12736.

9.   J. L. Corona-Guinto, L. Cardeño-García, D. C. Martínez-Casillas, J. M. Sandoval-Pineda, P. Tamayo-Meza, R. Silva-Casarin and R. G. González-Huerta, *Int. J. Hydrogen Energy*, 2013, **38**, 12667-12673.

10.   L. Gong, D. Ren, Y. Deng and B. S. Yeo, *ACS Appl. Mater. Interfaces*, 2016, **8**, 15985-15990.

11.   R. B. Moghaddam, C. Wang, J. B. Sorge, M. J. Brett and S. H. Bergens, *Electrochem. Commun.*, 2015, **60**, 109-112.

12.   Y. Pi, Q. Shao, X. Zhu and X. Huang, *ACS Nano*, 2018, **12**, 7371-7379.

13.   J.-M. Hu, J.-Q. Zhang and C.-N. Cao, *Int. J. Hydrogen Energy*, 2004, **29**, 791-797.

14.   J.-J. Zhang, J.-M. Hu, J.-Q. Zhang and C.-N. Cao, *Int. J. Hydrogen Energy*, 2011, **36**, 5218-5226.

15.   C. Massué, V. Pfeifer, X. Huang, J. Noack, A. Tarasov, S. Cap and R. Schlögl, *ChemSusChem*, 2017, **10**, 1943-1957.

16.   G. Li, S. Li, M. Xiao, J. Ge, C. Liu and W. Xing, *Nanoscale*, 2017, **9**, 9291-9298.

17.   P.-Y. Liu, C.-C. Hsu and M.-C. Chuang, *Journal of Materials Chemistry A*, 2017, **5**, 2959-2971.

18.   G. Li, S. Li, J. Ge, C. Liu and W. Xing, *Journal of Materials Chemistry A*, 2017, **5**, 17221-17229.

19.   L. Fu, P. Cai, G. Cheng and W. Luo, *Sustainable Energy & Fuels*, 2017, **1**, 1199-1203.

20.   L. C. Seitz, C. F. Dickens, K. Nishio, Y. Hikita, J. Montoya, A. Doyle, C. Kirk, A. Vojvodic, H. Y. Hwang and J. K. Norskov, *Science*, 2016, **353**, 1011-1014.

21.   M. Tariq, W. Q. Zaman, W. Sun, Z. Zhou, Y. Wu, L.-m. Cao and J. Yang, *ACS Sustainable Chemistry & Engineering*, 2018, **6**, 4854-4862.